Ukrainian Journal of Physical Optics
ISSUE 3
2026

WAKEFIELD ACCELERATION DRIVEN BY THE LASER PULSE WITH A STEEP FRONT IN VARIOUS PLASMA CHANNELS

D. S. BONDAR *, V. I. MASLOV, AND I. N. ONISHCHENKO

National Science Center "Kharkiv Institute of Physics and Technology", 1, Akademichna St., Kharkiv, 61108, Ukraine
*Corresponding author: bondar.ds@yahoo.com

Received: 23.03.2026

Abstract. Laser wakefield acceleration is an efficient method for generating and accelerating relativistic electron bunches. The parameters of these self-injected bunches depend on the laser and plasma parameters. In this paper, it is demonstrated that the formation of a self-injected bunch is sensitive to the profile of the driving laser pulse. The authors compared a steep-front pulse with a gradual-front pulse while keeping all other laser parameters identical. It is shown that a self-injected bunch forms for a steep front pulse, but no self-injection is observed for a gradual front pulse. The formation and subsequent wakefield acceleration of self-injected bunches were investigated in cylindrical and conical plasma channels for both homogeneous and longitudinally inhomogeneous plasma profiles. An increase in the energy of the self-injected bunch was achieved in the conical channel, as well as in the cylindrical channel with inhomogeneous plasma.

Keywords: laser, plasma channel, wakefield acceleration, inhomogeneous plasma, electron bunch
UDC: 533.9; 535.3; 519.6
DOI: 10.3116/16091833/Ukr.J.Phys.Opt.2026.03069

1. Introduction

Laser wakefield acceleration (LWFA) is a promising method for generating and accelerating relativistic electron bunches due to the extremely high accelerating gradients achievable in plasma [1, 2]. The basic physical principles of plasma acceleration using a laser-pulse driver and the main LWFA regimes have been discussed in many theoretical and review papers [2-10]. The development of high-power femtosecond laser systems has made LWFA experimentally accessible and attractive for compact accelerator applications, for which conventional radio-frequency structures are limited by dielectric breakdown [10]. Experimental demonstrations of monoenergetic and multi-GeV electron beams from compact laser-plasma accelerators have further confirmed the practical potential of this approach [11, 12].

An important feature of LWFA is the possibility of self-injection, when plasma electrons are trapped directly from the wakefield and then accelerated without the need for an externally injected bunch [1, 2]. At the same time, the formation of a self-injected bunch is highly sensitive to the laser and plasma parameters, because electron trapping depends on the wakefield structure and electron dynamics. These processes are nonlinear, self-consistent, the dynamics of one electron influences the dynamics of others. As a result, injection control remains one of the central problems of LWFA. And numerical simulation in this context is an effective method for investigation wakefield processes. In the present work, numerical simulations were performed using the WarpX code [13].

A number of approaches have been proposed to improve injection control and to increase the bunch energy. Multistage and hybrid acceleration schemes can overcome some limitations of

a single accelerating section, but they require multiple synchronized stages, separate targets, or additional preionization systems [14, 15]. Plasma methods (plasma lenses) are widely used as accelerator sections, including for focusing self-injected bunches [16-18]. Other modern approaches to improving the performance of laser-plasma accelerators include the use of uniform, high-density gas cells and dielectric structures. Such configurations can provide acceptable conditions for beam generation and acceleration, but they often remain sensitive to synchronization requirements and may still suffer from laser defocusing [19] and beam instability [20-24].

The formation and acceleration of self-injected bunches are studied by both the authors of the current paper and other authors. Studies of wakefield excitation in plasma often focus on electron trapping itself. In the paper [25], electron trapping was investigated experimentally, and stable electron beams with quasi-monoenergetic peaks in the 100 keV range were obtained. The low-power laser that can be used in this case (8 mJ) facilitates a high repetition rate (500 Hz). However, the authors use a downramp plasma density, which increases the number of captured electrons but, in this case, does not maintain the bunch in the wake-wave acceleration phase.

Previously, it was considered the formation of an entire self-injected electron bunch in high-density plasma [26]. This study focused on bunch dynamics and the maximum achievable acceleration field (2 TV/m) but was less focused on the bunch parameters. In [27], the dynamics of the self-injected bunch and its longitudinal momentum were investigated for a configuration that allowed the bunch to remain in the accelerating phase. Bunch acceleration was observed, but the prevention of laser pulse defocusing was not considered. Therefore, further optimization of the configuration was needed, in particular, by reducing the steepness of the plasma density gradient while saving the acceleration effect.

Since the acceleration distance is limited by laser pulse depletion and diffraction, authors of [28, 29] proposed a way to extend the acceleration distance by changing from acceleration driven only by the laser pulse to a combined (laser and plasma-based) acceleration regime. In the combined case, the leading bunches become drivers, generating their own wakefield that continues to efficiently accelerate the next self-injected bunches. This appears to be an effective approach. At the same time, as noted by the authors of [29], the beam quality achieved in this scheme still requires further improvement. Moreover, the problem of radial divergence in the laser driver remains an issue.

At the same time, cylindrical plasma channels and capillary discharge waveguides have been considered as ways to keep the laser pulse within the channel and prevent defocusing. In particular, guiding of laser pulses in hydrogen-filled capillary discharge waveguides was demonstrated in [30]. In related studies with preformed channels [31, 32], propagation of intense pulses over extended distances was investigated.

In this paper, conical channels are investigated as a means not only to preserve the laser pulse but also to focus it. In addition, the conical channel shape is used to prevent the wake bubble from expanding. Since the self-injected bunch propagates within the wake bubble structure, suppressing its expansion and the wake bubble's collapse leads to the decay of the self-injected bunch.

The temporal profile of the laser driver is a practically controllable parameter. Modern plasma-mirror techniques [33, 34] enable the generation of high-contrast ultrashort laser

pulses, thereby providing the experimental basis for forming a steep pulse front. In the present work, this possibility is used to initiate self-injection near threshold under otherwise identical laser parameters. The formed bunch is then further accelerated in cylindrical and conical plasma channels with homogeneous and inhomogeneous plasma.

Because of the earlier description and related studies, the general principle of increasing the energy of self-injected bunches, plasma channels, and a longitudinally increasing density gradient has usually been considered either separately or as parts of the system configuration, rather than as key factors directly influencing the bunch itself. Moreover, in studies of wakefield acceleration, the self-injection threshold (typically $a_0 \geq 2.0$) is usually exceeded by increasing the laser amplitude a_0.

In related studies, self-injection was typically achieved by increasing the laser amplitude above threshold, whereas the role of the laser front profile in near-threshold trapping has been insufficiently studied.

In the current paper, a different approach is considered. Self-injection is initiated not by increasing a_0, but by using a laser pulse with a steep front, with other laser parameters identical. The formed self-injected bunch is then accelerated in cylindrical and conical plasma channels with homogeneous and longitudinally inhomogeneous plasma profiles. Thus, the aim of the current paper is to investigate self-injection near threshold for different laser front profiles and to show how channel geometry and plasma inhomogeneity affect the acceleration and properties of the formed self-injected bunch.

2. Formation of a self-injected bunch in laser wakefield acceleration with a steep front laser driver

To study self-injection near the trapping threshold, 2D3V particle-in-cell (PIC) simulations were performed using the WarpX code [13]. The simulations were completed in Cartesian (x, z) geometry, where z is the laser propagation direction, and x is the transverse coordinate. The computational domain is rectangular. The laser pulse was initialized with a Gaussian transverse profile and a prescribed temporal envelope. Two temporal profiles (Fig. 1) were considered: a laser pulse with a gradual front and one with a steep front. In both cases, the laser wavelength, peak normalized amplitude a_0, was the same, where $a_0=eE_0(m_ec\omega_0)^{-1}$ (E_0 is the laser peak electric field amplitude, ω_0 - laser angular frequency), so that only the effect of the laser pulse front shape was compared.

The plasma density is normalized to the initial on-axis value, $n_{e0}=1.74\times10^{19}$ cm^{-3}; the value $n_e/n_{e0}=1$ in the figures corresponds to the initial uniform density on the axis. In the text, the normalized density is written as n_e/n_{e0}, while the label [n_{e0}] on the color scale indicates that the density values are given in units of n_{e0}. Spatial coordinates are given in units of $c/\omega_{pe}=1.27$ μm, where ω_{pe} is the electron plasma frequency (the characteristic plasma length scale). The laser wavelength is λ=800 nm ($\omega_0 = 2.36\times10^{15}$ rad/s), the waist is $w_0=4.05\ c/\omega_{pe}$, and the initial channel radius is $r_{ch}=4.15\ c/\omega_{pe}$. The pulse duration is $\tau_{full}=21.6$ fs. The simulation window is 142 c/ω_{pe} long and 12 c/ω_{pe} wide. The density at the channel walls is taken to be $10n_{e0}$.

For a laser pulse with a steep front, the ratio of the rise and fall times is $\tau_{rise}/\tau_{fall} = 1/7$. In both cases, the peak normalized amplitude is $a_0 = 2.15$. Figs. 2 and 3 show the plasma configurations considered in this work, namely cylindrical and conical plasma channels with homogeneous and inhomogeneous plasma profiles.

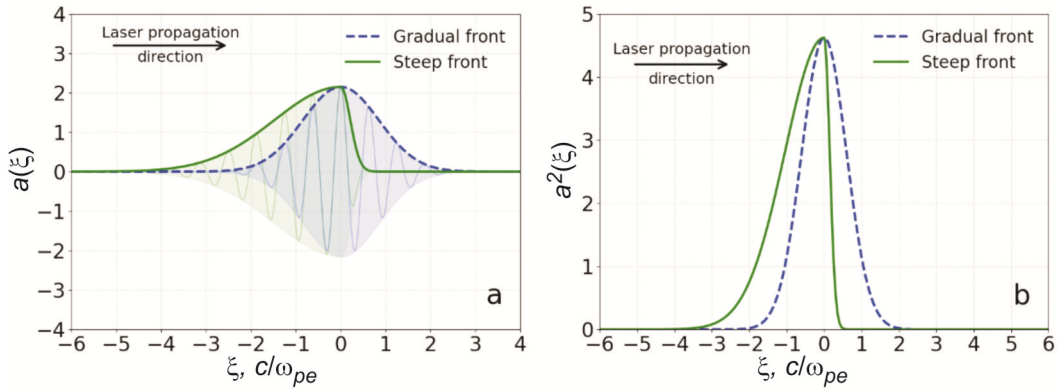

Fig. 1. Initial longitudinal profiles of the normalized laser vector potential in the co-moving coordinate $\xi=z-v_g t$: (a) $a(\xi)$ and (b) $a^2(\xi)$ for the gradual-front (blue dashed line) and steep-front (green solid line) laser pulses. Both pulses have the same peak normalized amplitude a_0=2.15. The ratio of the rise times is $\tau_{rise.\ Gradual.}$ / $\tau_{rise.\ Steep.}$ = 4. For a pulse propagating with the group velocity v_g, the temporal rise time τ_{rise} corresponds to the longitudinal front width $\Delta\xi_{rise}=v_g\tau_{rise}$. Therefore, $\tau_{rise.\ Gradual.}$ / $\tau_{rise.\ Steep.}$ = 4 means that the front region of the laser pulse gradual front is 4 times wider in ξ than that of the steep-front pulse.

In Figs. 2 and 3 the color map represents the 2D normalized distribution $n_e(z, x)/n_{e0}$. The blue curve, referenced to the blue right vertical axis, shows the on-axis longitudinal density profile $n_e(z, x=0)/n_{e0}$. Thus, panel (a) corresponds to a homogeneous plasma profile, whereas panel (b) shows a longitudinally inhomogeneous profile.

A remark needs to be made about the laser pulse with a steep front discussed in the current paper. Experimentally, such a front can be realized using temporal-contrast cleaning techniques, most commonly plasma mirrors [33, 34].

In this paper, a two-dimensional geometry is used as a comparative numerical model to identify the roles of the laser front profile and plasma channel configurations. In such a formulation, the main features of wakefield formation, electron trapping, and the relative effects of changes in the channel geometry and plasma profile are clearly resolved. At the same time, some quantitative characteristics may depend on the model's dimensionality. For this reason, the present study focuses on the comparative trends revealed between cases calculated under the same numerical conditions.

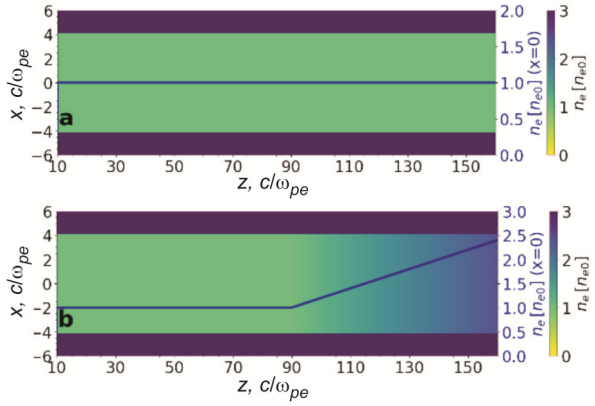

Fig. 2. Initial plasma-density distributions $n_e(z, x)$ in a cylindrical plasma channel: (a) homogeneous plasma channel; (b) cylindrical plasma channel with longitudinally inhomogeneous plasma. The color map shows the normalized density distribution $n_e(z, x)/n_{e0}$ in the (z, x) plane. The blue curve, read from the blue right-hand vertical axis, shows the on-axis longitudinal density profile $n_e(z, x=0)/n_{e0}$. In panel (a), this profile is constant, but in panel (b) it increases along z. The laser and self-injected bunches in these configurations move from left to right.

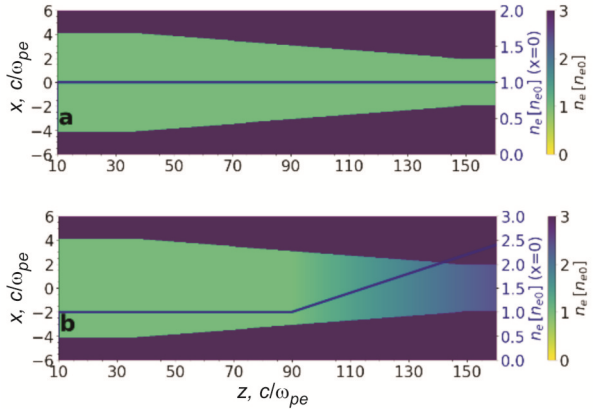

Fig. 3. Initial plasma-density distributions $n_e(z, x)$ in a conical plasma channel: (a) homogeneous plasma channel; (b) conical plasma channel with longitudinally inhomogeneous plasma. The color map shows the normalized density distribution $n_e(z, x)/n_{e0}$ in the (z, x) plane. The blue curve, read from the blue right-hand vertical axis, shows the on-axis longitudinal density profile $n_e(z, x=0)/n_{e0}$. In panel (a), this profile is constant, whereas in panel (b) it increases along z. The laser and self-injected bunches in these configurations move from left to right

The self-injected bunch sizes are the maximum longitudinal size (Length) in the z-direction and the maximum transverse size (Width) in the x-direction. The bunch size is characterized by its 2D area, defined by its length×width (S_b [μm²]). The criterion for a small bunch was set at $S_b \leq 1$ μm².

The characteristics of the self-injected electron bunch were determined through statistical analysis of the macroparticle data. Since the statistical weights of all macroparticles were equal, the mean energy of the bunch was calculated by directly averaging the total relativistic energies of the individual particles, $\langle E\rangle=\langle\gamma\rangle m_e c^2$. For the obtained highly relativistic bunches ($p_z \gg p_x$ and $p_z \gg m_e c$), the Lorentz factor can be approximated as $\gamma \approx p_z/(m_e c)$, and therefore $\langle\gamma\rangle \approx \langle p_z\rangle/(m_e c)$. Particular attention was given to the transverse quality of the bunch.

The transverse bunch quality was completed using the RMS emittance. For this purpose, a classical phase-space calculation was performed. The geometric emittance was calculated based on the transverse coordinates of the particles and their divergence angles $x' = \arctan(p_x / p_z)$:

$$\varepsilon_x = \sqrt{\left\langle \left(x - \langle x\rangle\right)^2 \right\rangle \left\langle \left(x' - \langle x'\rangle\right)^2 \right\rangle - \left\langle \left(x - \langle x\rangle\right)\left(x' - \langle x'\rangle\right) \right\rangle^2} \quad . \tag{1}$$

Here, ε_x is the geometric RMS emittance, x is the transverse coordinate, and x' is the particle divergence angle in the (x, z) plane. Eq (1) is the standard statistical phase space expression for the RMS emittance and is based on the second moments of the beam distribution: the RMS beam size, the RMS angular spread, and the correlation between the transverse position and the divergence angle.

The quantity shown in Fig. 4 was obtained from the initial longitudinal profiles $a^2(\xi)$ presented in Fig. 1b by calculating the derivative $-\partial a^2/\partial\xi$. This quantity is proportional to the longitudinal ponderomotive force averaged over the laser cycle and therefore characterizes the steepness of the laser pulse front.

The ponderomotive force F_z drives the electron displacement and wakefield excitation, and is proportional to the longitudinal derivative of the squared normalized vector potential $a^2(\xi)$.

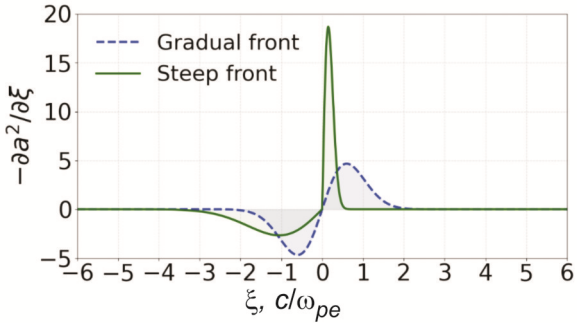

Fig. 4. Profiles of the quantity $-\partial a^2/\partial\xi$ for the laser pulses with a gradual and a steep front, calculated from the initial longitudinal profiles $a^2(\xi)$. This quantity is proportional to the longitudinal ponderomotive force F_z.

The longitudinal ponderomotive force acting on plasma electrons is determined by the gradient of the ponderomotive potential:

$$F_z = -\frac{\partial U_p}{\partial z}. \tag{2}$$

Using the standard relation between the normalized laser amplitude and the electron quiver motion, the relativistic ponderomotive potential can be written as $U_p = m_e c^2(\bar{\gamma} - 1)$. For a linearly polarized laser field, after averaging over the fast laser oscillation, the relativistic factor averaged over the laser cycle becomes $\bar{\gamma} = \sqrt{1 + a^2/2}$ [2], which gives:

$$U_p = m_e c^2\left(\sqrt{1 + \frac{a^2}{2}} - 1\right), \tag{3}$$

Where $a = a(\xi)$ is the dimensionless normalized laser amplitude defined above, a_0 is the peak value of a. By differentiating Eq. (3) with respect to z, the following expression is obtained:

$$F_z = -m_e c^2 \frac{1}{4\sqrt{1 + a^2/2}} \frac{\partial a^2}{\partial z}. \tag{4}$$

Since $\xi = z - v_g t$, at a fixed time t:

$$\frac{\partial}{\partial z} = \frac{\partial}{\partial \xi}$$

When two pulses with the same peak amplitude a_0 are compared, the factor is $1/\sqrt{1 + a^2/2}$ identical in both cases and does not affect their ratio. Therefore, the ponderomotive force is determined by the gradient:

$$F_z(\xi) \propto -\frac{\partial a^2(\xi)}{\partial \xi}, . \tag{5}$$

Thus, the derivative $\partial a^2/\partial\xi$ of the squared normalized vector potential with respect to the co-moving coordinate characterizes the steepness of the pulse front. For laser pulses with the same peak amplitude a_0, the maximum ponderomotive force can be estimated from the characteristic front length L_{front}. Let $s = \xi / L_{front}$ be the dimensionless longitudinal coordinate across the pulse front. In this representation, a_0 sets the peak amplitude, L_{front} defines the characteristic front length, and the dimensionless function $f(s)$ describes only the front shape. Then the laser envelope can be written as:

$$a(\xi) = a_0 f\left(\frac{\xi}{L_{front}}\right) = a_0 f(s), 0 \le s \le 1, \tag{6}$$

where f is a dimensionless shape function normalized so that $f=1$ at the pulse peak and $f=0$ ahead of the pulse and $s=\xi/L_{front}$ is the dimensionless longitudinal coordinate across the pulse front. From Eq. (6), squaring both sides gives $a^2=a_0^2 f^2(s)$. Differentiating with respect to ξ by the chain rule, $\frac{\partial}{\partial\xi}=\frac{1}{L_{front}}\frac{d}{ds}$ it can be obtained:

$$\frac{\partial a^2}{\partial\xi}=\frac{a_0^2}{L_{front}}\frac{df^2}{ds}. \tag{7}$$

This result can be verified directly: since $a^2=a_0^2 f^2(s)$ and $s=\xi/L_{front}$, applying the chain rule gives $\partial a^2/\partial\xi=a_0^2\cdot(df^2/ds)\cdot(ds/d\xi)=\left(a_0^2/L_{front}\right)\left(df^2/ds\right)$. The maximum of the derivative can be written as:

$$\left|\frac{\partial a^2}{\partial\xi}\right|_{\max}=\frac{a_0^2}{L_{front}}\max\left|\frac{\partial f^2}{\partial s}\right| \tag{8}$$

For the two profiles shown in Fig. 1, the dimensionless coefficient

$$C_f=\max\left|\frac{\partial f^2}{\partial s}\right|$$

is a shape factor of order unity. Therefore, for comparable normalized front shapes, the leading dependence of the maximum gradient is determined by L_{front}, i.e.

$$\left|\frac{\partial a^2}{\partial\xi}\right|_{\max}\propto\frac{a_0^2}{L_{front}} \tag{9}$$

Assuming that the front length is related to the rise time by $L_{front}\approx v_g\tau_{rise}$, it can be obtained:

$$\left|\frac{\partial a^2}{\partial\xi}\right|_{\max}\propto\frac{a_0^2}{v_g\tau_{rise}} \tag{10}$$

Thus, for two laser pulses with identical peak amplitude a_0 propagating in the same plasma, the ratio of the maximum longitudinal ponderomotive forces is

$$\frac{F_{Steep}}{F_{Gradual}}\approx\frac{\left|\partial a^2/\partial\xi\right|_{\max,Steep}}{\left|\partial a^2/\partial\xi\right|_{\max,Gradual}}\approx\frac{a_0^2/\left(v_g\tau_{rise,Steep}\right)}{a_0^2/\left(v_g\tau_{rise,Gradual}\right)}=\frac{\tau_{rise,Gradual}}{\tau_{rise,Steep}}. \tag{11}$$

In the present case,

$$\frac{\tau_{rise,Gradual}}{\tau_{rise,Steep}}=4\Rightarrow\frac{F_{Steep}}{F_{Gradual}}\approx 4. \tag{12}$$

This scaling estimate indicates the expected difference between the two driver laser pulses. For laser pulses with the same peak amplitude a_0 propagating in the same plasma, the characteristic maximum longitudinal ponderomotive force increases as the rise time decreases. Therefore, for the laser pulse profiles considered here, where $\tau_{rise,Gradual}/\tau_{rise,Steep}$ = 4, the laser pulse with a steep front is expected to provide a stronger longitudinal ponderomotive drive than the laser pulse with a gradual front. Since self-injection is a nonlinear process, the actual effect of electron trapping needs to be determined from PIC simulations rather than from scaling estimates alone.

To compare the wakefield structure of the two laser pulse profiles, the normalized plasma density distribution, $n_e(z, x)/n_{e0}$, and the on-axis accelerating field are shown next. In

the current paper, the accelerating field refers to the longitudinal electric field component E_z on the channel axis, $E_z(z, x=0)$, which is responsible for accelerating trapped electrons. In these plots, the color map shows $n_e(z, x)/n_{e0}$, while the red curve, referenced to the right vertical axis, shows $E_z(z, x=0)$.

Figs. 5 and 6 show the wakefield structure in the homogeneous cylindrical channel at the same propagation time (t=342.1 fs) for the two laser pulses profile. In both figures, the color map represents the normalized plasma density distribution $n_e(z, x)/n_{e0}$, while the red curve shows the on-axis accelerating field $E_z(z, x=0)$, referenced to the right vertical axis.

In the case of the laser pulse with a gradual front (Fig. 5), no compact self-injected bunch forms in the rear of the wake bubble. In contrast, for the laser pulse with a steep front (Fig. 6), a clear compact self-injected electron bunch appears near the back of the bubble, in the accelerating phase of the wakefield. Therefore, keeping all other laser and plasma parameters constant, modifying only the laser front profile leads to electron trapping and self-injected bunch formation in the threshold case, a_0=2.15.

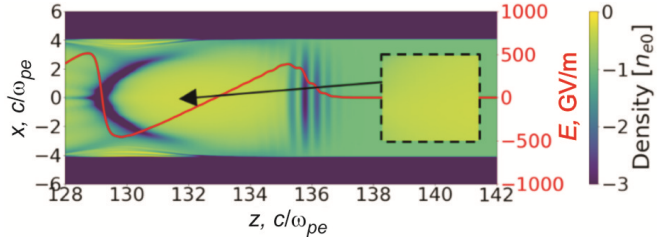

Fig. 5. Normalized plasma density distribution $n_e(z, x)/n_{e0}$ (color map) and on-axis accelerating field $E_z(z, x=0)$ (red curve, right vertical axis) in the **cylindrical channel with longitudinally *homogeneous* plasma** at t=342.1 fs for the laser pulse with a **gradual front**. No formed self-injected bunch is observed.

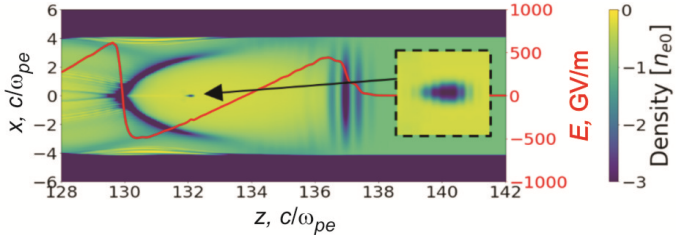

Fig. 6. Normalized plasma density distribution $n_e(z, x)/n_{e0}$ (color map) and on-axis accelerating field $E_z(z, x=0)$ (red curve, right vertical axis) in the **cylindrical channel with longitudinally *homogeneous* plasma** at t=342.1 fs for the laser pulse with **steep front**. A compact self-injected electron bunch is formed near the rear part of the wake bubble.

3. Acceleration of a self-injected bunch formed in the wake acceleration with a steep front laser pulse driver

The Wakefield structures and the formed self-injected electron bunches for the laser pulse with a steep front are shown in Figs. 7-9 for the cylindrical channel with longitudinally inhomogeneous plasma and for the conical channels with homogeneous and longitudinally inhomogeneous plasma. Table 1 summarizes the parameters of these self-injected bunches. Analysis of the presented results shows that the proposed LWFA scheme, when the laser driver has a steep front, initiates self-injection, whereas with a gradual front, self-injection is absent under the same parameters *across all configurations*. The results also demonstrate several ways to increase the longitudinal momentum of the formed self-injected bunch. This is achieved using a conical channel, longitudinal plasma inhomogeneity, or both.

Relatively small changes in density (from $1{\cdot}n_{e0}$ to $2{\cdot}n_{e0}$) and channel radius (from

4.15 c/ω_{pe} to 2.29 c/ω_{pe}) were considered to prevent the defocusing and decay of the self-injected bunch, as well as to avoid inhomogeneous acceleration of the bunch front and tail. The data presented in Table 1 demonstrates how both the plasma channel geometry and the density profile determine the properties of the injected electron bunch.

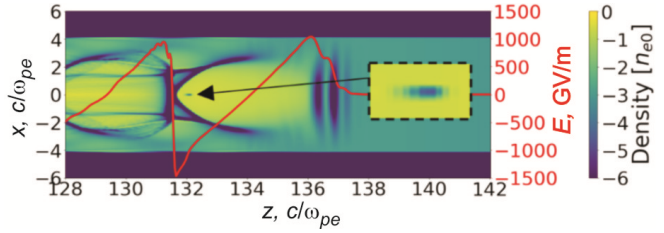

Fig. 7. Normalized plasma density distribution $n_e(z, x)/n_{e0}$ (color map) and on-axis accelerating field $E_z(z, x=0)$ (red curve, right vertical axis) in the **cylindrical channel with longitudinally *inhomogeneous* plasma** at t=342.1 fs for the laser pulse with **steep front**. A self-injected electron bunch is observed near the rear part of the wake bubble.

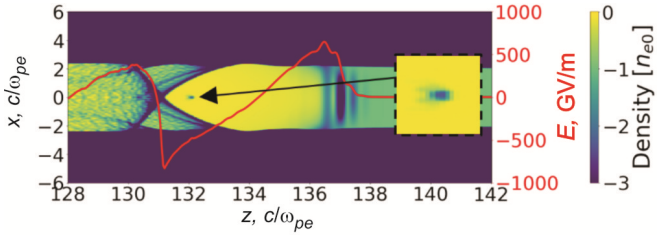

Fig. 8. Normalized plasma density distribution $n_e(z, x)/n_{e0}$ (color map) and on-axis accelerating field $E_z(z, x=0)$ (red curve, right vertical axis) in the **conical channel with longitudinally *homogeneous* plasma** at t=342.1 fs for the laser pulse with **steep front**. A self-injected electron bunch is observed near the rear part of the wake bubble.

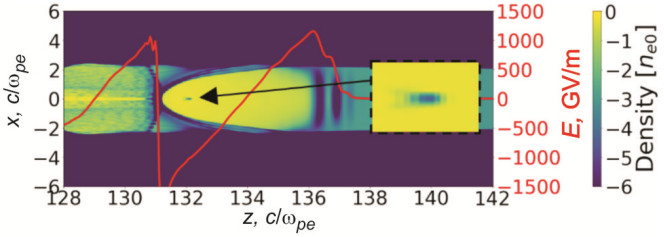

Fig. 9. Normalized plasma density distribution $n_e(z, x)/n_{e0}$ (color map) and on-axis accelerating field $E_z(z, x=0)$ (red curve, right vertical axis) in the **conical channel with longitudinally *inhomogeneous* plasma** at t=342.1 fs for the laser pulse with **steep front**. A self-injected electron bunch is observed near the rear part of the wake bubble.

Table 1. Parameters of self-injected bunches. Steep front laser pulse profile.

Parameter	Cylindrical channel		Conical channel	
	Hom.	Inh.	Hom.	Inh.
Longitudinal size of the bunch, μm	0.65	0.70	1.03	0.91
Transverse size of the bunch, μm	0.42	0.49	0.83	0.62
S_b (2D), μm^2	0.273	0.343	0.855	0.564
$<p_z>$, m_ec	97.11	116.87	106.86	128.13
Std. deviation $<p_z>$, m_ec	2.03 (2.1%)	3.23(2.8%)	0.54(0.5%)	3.55(2.8%)
Emittance, mm×mrad	7.5×10^{-4}	7.5×10^{-4}	2.1×10^{-4}	9.0×10^{-4}
Mean energy, MeV	49.6	59.7	54.6	65.5

The maximum accelerating field E_z increases from 291 GV/m in the homogeneous cylindrical channel to 626 GV/m in the inhomogeneous cylindrical channel, 478 GV/m in the homogeneous conical channel, and reaches its highest value of 769 GV/m in the inhomogeneous conical channel.

For the ultrarelativistic bunches considered in this paper, the mean energy values are consistent with the corresponding mean longitudinal momentum values, because the total momentum is dominated by its longitudinal component, $p \approx p_z$, so that $\gamma \approx p_z/(m_e c)$ and, consequently, $\langle E \rangle = \langle \gamma \rangle m_e c^2 \approx \langle p_z \rangle c$.

Comparison of conical geometry in the inhomogeneous case and cylindrical geometry in the homogeneous case. The main result shown in this section is the combined effect of the conical geometry, which prevents the laser pulse from expanding radially and focuses it, and the longitudinally inhomogeneous plasma, which, together with the conical geometry, keeps the self-injected bunch in the wake-wave acceleration phase. An increase in the bunch energy by 32.1% (from 49.6 MeV to 65.5 MeV) is observed. The standard deviation of the p_z increases slightly (by 0.7%). The emittance and area of the bunch increase, but the emittance remains $<1\times10^{-3}$ mm×mrad, and the bunch area <1 μm^2.

Comparison of conical and cylindrical geometry in the homogeneous case. In the homogeneous conical channel a larger bunch was formed (0.855 μm^2 in the conical case and 0.273 μm^2 for the cylindrical channel) while simultaneously providing better bunch quality: the emittance is reduced to 2.1×10^{-4} mm×mrad and the relative momentum spread reaches 0.5%, compared with 7.5×10^{-4} mm×mrad and 2.1% in the cylindrical configuration. The conical geometry also maintains a higher accelerating field ($E_{z,max}$ = 478 GV/m in conical case, and 291 GV/m in cylindrical case), which gives higher momentum and energy (p_z = 106.86 m_ec, energy = 54.6 MeV) relative to the homogeneous cylindrical case (97.11 m_ec, 49.6 MeV).

Comparison of conical and cylindrical geometry in the inhomogeneous case. When the plasma density is inhomogeneous, both geometries show a significant increase in wakefield amplitude and energy gain compared with homogeneous plasma. The cylindrical channel increases to $E_{z,max}$ = 626 GV/m and mean energy = 59.7 MeV, while in the case of the conical channel, the amplitude reaches the highest value, $E_{z,max}$ = 769 GV/m, the mean energy is 65.5 MeV, and p_z=128.13 m_ec. The corresponding bunch sizes show a moderate adjustment: in the cylindrical case, bunches become slightly larger (0.343 μm^2), whereas in the conical case, they become 64.4% compact (0.564 μm^2) under a stronger accelerating field. The length of the accelerating interval was 98.4 μm for all cases. Fig. 10 shows the longitudinal momentum p_z of the self-injected bunches for the considered configurations.

The results show that the self-injected bunch maintains its transverse compactness and avoids radial spreading during propagation across all considered setups (Fig. 10).

Fig. 11 shows a graph of laser pulse energy density in cylindrical and conical channels. It can be observed that the laser pulse radius is reduced by a factor of 2 in the case of a conical channel.

The maximum energy density on the x=0 axis is 0.65 PJ/m^3 in the cylindrical channel and 1.1 PJ/m^3 in the conical channel (Fig. 11). In the conical channel, radial laser focusing not only keeps the pulse inside the channel but also increases the maximum on-axis energy density by 69.2% relative to the cylindrical case.

For the cases considered in this paper, the bunch charge ranged from 1 to 4 pC. It was obtained from the simulation results data. This charge range is practically relevant for applications based on diffraction and imaging with MeV electrons [35, 36].

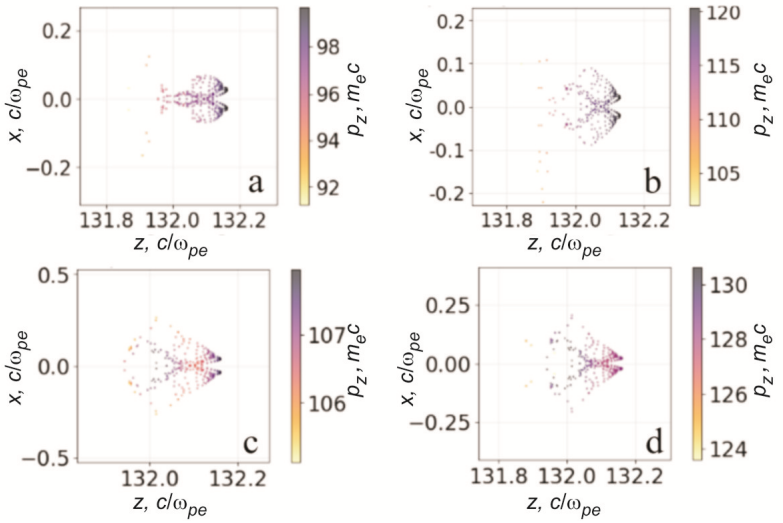

Fig. 10. Longitudinal momentum $p_z(z, x)$. Cylindrical channel: a) homogeneous plasma, b) inhomogeneous plasma profile. Conical channel: c) homogeneous plasma profile, d) inhomogeneous plasma profile. t=342.1 fs. Steep front laser pulse profile.

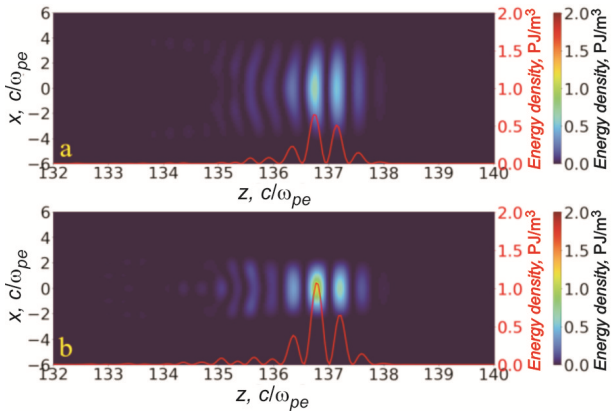

Fig. 11. Energy density of the laser pulse: (a) cylindrical channel, (b) conical channel. The color map shows the 2D energy density distribution, and the red line shows the energy density profile on the system axis x=0).

A comparison can be made with the experimental studies [37, 38], since they describe injection-sensitive LWFA regimes with measured bunch parameters. In [37], quasimonoenergetic electron bunches with energies up to 15 MeV, a charge of about 2.5 pC, and a divergence below 7 mrad were reported, while in [38] stable self-injected bunches with a peak energy of about 36 MeV, a charge of about 4 pC, and a divergence on the order of 10 mrad were obtained. In this paper, the authors present bunch energies ranging from 49.6 to 65.5 MeV for bunch charges of 1-4 pC, with the highest value obtained in the longitudinally inhomogeneous conical channel. Thus, even the lowest-energy bunches obtained in the present paper exceed the maximum energy reported in [37] several times, with emittance on the order of 10^{-3} mm×mrad, while the best simulated case is also higher than the level achieved in [38]. This interpretation is also consistent with published simulations. In [39], PIC simulations showed that small density ripples as short as about 50 μm are sufficient to trigger self-injection at a_0=2.2, whereas below this threshold, injection is absent. In the present work, a similar near-threshold sensitivity is observed: at a_0=2.15, a pulse with a steep front leads to self-injection,

whereas a pulse with a gradual front does not under the same conditions. In addition, the PIC study of sharp density transitions in [40] predicted additional energy gain relative to the reference case, which is consistent with the increase in mean bunch energy obtained in the present paper for the longitudinally inhomogeneous conical channel compared with the homogeneous cylindrical channel. The results indicate that initiating self-injection by a steep-front laser pulse and then accelerating the bunch in a plasma channel can be an effective way to increase electron energy while keeping the bunch charge in the picocoulomb range.

The present results were obtained in 2D, so some quantitative values may depend on the model's dimensionality. In particular, the self-injection threshold, transverse focusing, emittance, and beam divergence may differ slightly in a fully 3D description. At the same time, 2D particle-in-cell simulations are widely used in laser wakefield acceleration studies [25, 41]. Moreover, in [25], qualitatively identical results were obtained in 2D and 3D simulations for the relevant injection dynamics. In the present work, however, the use of a 2D geometry does not affect the main comparative conclusions, because all cases were calculated within the same numerical model and under the same basic laser and plasma parameters. Therefore, the observed differences in self-injection and bunch acceleration are determined by the laser pulse front shape and the plasma configuration rather than by the dimensionality itself.

4. Conclusions

In contrast to previous studies, the current paper shows that self-injection near threshold can be obtained by changing the temporal front profile of the laser pulse, without increasing the laser pulse's peak normalized amplitude. In addition, the present work analyzes not only the formation of a self-injected bunch, but also its acceleration in cylindrical and conical plasma channels with both homogeneous and longitudinally inhomogeneous plasma profiles. Among the considered configurations, the combination of a laser pulse with a steep front, conical channel geometry, and longitudinal plasma inhomogeneity provides the highest accelerating field and the highest bunch energy.

The combined effect of the conical geometry and the longitudinal density gradient increases the maximum accelerating field from 291 GV/m to 769 GV/m compared with a homogeneous cylindrical channel. This leads to a 32.1% increase in the mean bunch energy, rising from 49.6 MeV to 65.5 MeV. The longitudinal momentum increases from 97.11 $m_e c$ to 128.13 $m_e c$.

The conical channel also prevents radial laser expansion, thereby focusing the pulse and increasing the maximum energy density on the axis by 69.2% while reducing the laser pulse radius to 50% of its initial value.

Funding and acknowledgments. The study is supported by the National Research Foundation of Ukraine under the program “Excellent Science in Ukraine” (project # 2023.03/0182).

Disclosures. The authors declare no conflicts of interest.

Authors contribution. D. S. Bondar contributed to the study concept, developed the methodology, performed the simulations, analyzed the results, and prepared the first draft of the paper. V. I. Maslov contributed to the study concept, the analysis of the results, and paper editing. I. N. Onishchenko supervised the work, contributed to the analysis, discussion of the results, and to paper editing.

References

1. Tajima, T., & Dawson, J. M. (1979). Laser electron accelerator. *Physical Review Letters*, *43*(4), 267.
2. Esarey, E., & Schroeder, C. B. (2003). *Physics of laser-driven plasma-based accelerators* (No. LBNL--53510). Ernest Orlando Lawrence Berkeley National Laboratory, Berkeley, CA (United States).
3. Ting, A. C. (1999, June). Ultra-high gradient acceleration of electrons by laser wakefield plasma waves. In *IEEE Conference Record-Abstracts. 1999 IEEE International Conference on Plasma Science. 26th IEEE International Conference (Cat. No. 99CH36297)* (p. 153). IEEE.
4. Onishchenko, I. N. (2006). Wakefield acceleration based on high power pulsed lasers and electron beams (overview). *Problems of Atomic Science and Technology. Series "Nuclear Physics Investigations*, (2), 46.
5. Tajima, T. (2014). Laser acceleration in novel media. *The European Physical Journal Special Topics*, *223*(6), 1037-1044.
6. Maslov, V. I., Bondar, D. S., Levchuk, I. P., Onishchenko, I. N., & Ovsiannikov, R. T. (2021). Plateau formation on accelerating wakefield for electron-witness-bunch and on decelerating wakefield for driver-bunches in a plasma. *Problems of Atomic Science and Technology*, *136*(6), 52-56.
7. Bondar, D. S., Maslov, V. I., & Onishchenko, I. N. (2023). A method for maintaining the acceleration rate and increasing the energy of self-injected bunch due to the use of inhomogeneous plasma. *Problems of Atomic Science and Technology*, *4*, 67-71.
8. Maslov, V. I., Bondar, D. S., Grigorencko, V., Levchuk, I. P., & Onishchenko, I. N. (2020). Control of characteristics of self-injected and accelerated electron bunch in plasma by laser pulse shaping on radius, intensity and shape. *arXiv preprint arXiv:2009.04816*.
9. Lindstrøm, C. A., Garland, J. M., Schröder, S., Boulton, L., Boyle, G., Chappell, J., D'Arcy, R. & Osterhoff, J. (2021). Energy-spread preservation and high efficiency in a plasma-wakefield accelerator. *Physical Review Letters*, *126*(1), 014801.
10. Hooker, S. M. (2013). Developments in laser-driven plasma accelerators. *Nature Photonics*, *7*(10), 775-782.
11. Leemans, W. P., Nagler, B., Gonsalves, A. J., Tóth, C., Nakamura, K., Geddes, C. G., … & Hooker, S. M. (2006). GeV electron beams from a centimetre-scale accelerator. *Nature Physics*, *2*(10), 696-699.
12. Mangles, S. P., Murphy, C. D., Najmudin, Z., Thomas, A. G. R., Collier, J. L., Dangor, A. E., Divall, … & Krushelnick, K. (2004). Monoenergetic beams of relativistic electrons from intense laser–plasma interactions. *Nature*, *431*(7008), 535-538.
13. Fonseca, R. A., Vieira, J., Fiúza, F., Davidson, A., Tsung, F. S., Mori, W. B., & Silva, L. O. (2013). Exploiting multi-scale parallelism for large scale numerical modelling of laser wakefield accelerators. *Plasma Physics and Controlled Fusion*, *55*(12), 124011.
14. Steinke, S., Van Tilborg, J., Benedetti, C., Geddes, C. G. R., Schroeder, C. B., Daniels, J., … & Leemans, W. P. (2016). Multistage coupling of independent laser-plasma accelerators. *Nature*, *530*(7589), 190-193.
15. Kurz, T., Heinemann, T., Gilljohann, M. F., Chang, Y. Y., Couperus Cabadağ, J. P., Debus, A., ... & Irman, A. (2021). Demonstration of a compact plasma accelerator powered by laser-accelerated electron beams. *Nature Communications*, *12*(1), 2895.
16. Sjobak, K. N., Adli, E., Corsini, R., Farabolini, W., Boyle, G., Lindstrøm, C. A., ... & Dyson, A. E. (2021). Strong focusing gradient in a linear active plasma lens. *Physical Review Accelerators and Beams*, *24*(12), 121306.
17. Maslov, V. I., Onishchenko, I. N., & Yarovaya, I. P. (2013). Plasma wakefield excitation providing homogeneous focusing of electron bunches. *Problems of Atomic Science and Technology*, *1*, 134.
18. Levchuk, I. P., Maslov, V. I., & Onishchenko, I. N. (2016). Focusing by wakefield and plasma focusing of relativistic electrons in dependence on parameters of experiments. *Problems of Atomic Science and Technology*, *103*(3), 62-65.
19. Sotnikov, G. V., Vasiliev, A. V., Beznosenko, I. V., Kovalov, S. M., Povrozin, A. I., & Svystunov, O. O. (2025). Comparative analysis of electron acceleration by laser pulse in flat and grating dielectric structures. *Nuclear Instruments and Methods in Physics Research Section A: Accelerators, Spectrometers, Detectors and Associated Equipment*, *1072*, 170158.
20. Martinez de la Ossa, A., Mehrling, T. J., & Osterhoff, J. (2018). Intrinsic stabilization of the drive beam in plasma-wakefield accelerators. *Physical Review Letters*, *121*(6), 064803.
21. Mehrling, T. J., Fonseca, R. A., Martinez De La Ossa, A., & Vieira, J. (2017). Mitigation of the hose instability in plasma-wakefield accelerators. *Physical Review Letters*, *118*(17), 174801.
22. Finnerud, O. G., Lindstrøm, C. A., & Adli, E. (2025). Parametric mapping of the efficiency-instability relation in plasma-wakefield accelerators. *Physical Review Accelerators and Beams*, 28(7), 071301.
23. Demydenko, I. V., Maslov, V. I., & Onishchenko, I. M. (2025). Suppression of bunch destruction under resonant excitation of the plasma wakefield. *Nuclear Instruments and Methods in Physics Research Section A: Accelerators, Spectrometers, Detectors and Associated Equipment*, 170851.
24. Demydenko, I. V., & Maslov, V. I. (2025). Electron Acceleration by a Wakefield Excited in Plasma by a Profiled Train of Bunches Under Conditions of Their Greatest Stability and a Plateau on the Wakefield. *IEEE Transactions on Plasma Science*, *54*(1), 117-120.
25. He, Z. H., Hou, B., Nees, J. A., Easter, J. H., Faure, J., Krushelnick, K., & Thomas, A. G. R. (2013). High repetition-rate wakefield electron source generated by few-millijoule, 30 fs laser pulses on a density downramp. *New Journal of Physics*, *15*(5), 053016.

26. Bondar, D., Maslov, V., Levchuk, I., & Onishcenko, I. (2020). Extitation of wakefield by a laser pulse in a metallic-density electron plasma. *arXiv preprint arXiv:2001.01246*.
27. Maslov, V. I., Bondar, D. S., & Onishchenko, I. N. (2022, March). Investigation of the way of phase synchronization of a self-injected bunch and an accelerating wakefield in solid-state plasma. In *Photonics* (Vol. 9, No. 3, p. 174). MDPI.
28. Maslov, V. I., Svystun, O. M., Onishchenko, I. N., & Yegorov, A. M. (2016). Joint wakefield acceleration by laser pulse and by self-injected electron bunches. *Problems of Atomic Science and Technology*, *6*, 144.
29. Maslov, V. I., Svystun, O. M., Onishchenko, I. N., & Tkachenko, V. I. (2016). Dynamics of electron bunches at the laser–plasma interaction in the bubble regime. *Nuclear Instruments and Methods in Physics Research Section A: Accelerators, Spectrometers, Detectors and Associated Equipment*, *829*, 422-425.
30. Butler, A., Spence, D. J., & Hooker, S. M. (2002). Guiding of high-intensity laser pulses with a hydrogen-filled capillary discharge waveguide. *Physical Review Letters*, *89*(18), 185003.
31. Geddes, C. G. R., Toth, C., Van Tilborg, J., Esarey, E., Schroeder, C. B., Bruhwiler, D., ... & Leemans, W. P. (2004). High-quality electron beams from a laser wakefield accelerator using plasma-channel guiding. *Nature*, *431*(7008), 538-541.
32. Geddes, C. G. R., Toth, C., Van Tilborg, J., Esarey, E., Schroeder, C. B., Cary, J., & Leemans, W. P. (2005). Guiding of relativistic laser pulses by preformed plasma channels. *Physical Review Letters*, *95*(14), 145002.
33. Dromey, B., Kar, S., Zepf, M., & Foster, P. J. R. O. S. I. (2004). The plasma mirror—a subpicosecond optical switch for ultrahigh power lasers. *Review of Scientific Instruments*, *75*(3), 645-649.
34. Lévy, A., Ceccotti, T., d'Oliveira, P., Réau, F., Perdrix, M., Quéré, F., ... & Audebert, P. (2007). Double plasma mirror for ultrahigh temporal contrast ultraintense laser pulses. *Optics letters*, *32*(3), 310-312.
35. Li, R. K., & Musumeci, P. (2014). Single-shot MeV transmission electron microscopy with picosecond temporal resolution. *Physical Review Applied*, *2*(2), 024003.
36. Yang, J., Kan, K., Tanimura, K., Yoshida, Y., & Urakawa, J. (2016). Ultrafast electron microscopy using 100 femtosecond relativistic-energy electron beam. *Proc. of IPAC2016, Busan, Korea*, 3183-3185.
37. Salehi, F., Le, M., Railing, L., Kolesik, M., & Milchberg, H. M. (2021). Laser-accelerated, low-divergence 15-MeV quasimonoenergetic electron bunches at 1 kHz. *Physical Review X*, *11*(2), 021055.
38. Rao, B. S., Moorti, A., Rathore, R., Chakera, J. A., Naik, P. A., & Gupta, P. D. (2014). High-quality stable electron beams from laser wakefield acceleration in high density plasma. *Physical Review Special Topics-Accelerators and Beams*, *17*(1), 011301.
39. Kuschel, S., Schwab, M. B., Yeung, M., Hollatz, D., Seidel, A., Ziegler, W., ... & Zepf, M. (2018). Controlling the self-injection threshold in laser wakefield accelerators. *Physical Review Letters*, *121*(15), 154801.
40. Döpp, A., Guillaume, E., Thaury, C., Lifschitz, A., Ta Phuoc, K., & Malka, V. (2016). Energy boost in laser wakefield accelerators using sharp density transitions. *Physics of Plasmas*, *23*(5).
41. Geddes, C. G. R., Nakamura, K., Plateau, G. R., Toth, C., Cormier-Michel, E., Esarey, E., ... & Leemans, W. P. (2008). Plasma-density-gradient injection of low absolute-momentum-spread electron bunches. *Physical Review Letters*, *100*(21), 215004.

Bondar, D. S., Maslov, V. I., and Onishchenko, I. N. (2026). Wakefield Acceleration Driven by the Laser Pulse with a Steep Front in Various Plasma Channels**.** *Ukrainian Journal of Physical Optics*, *27*(3), 03069 – 03082. doi: 10.3116/16091833/Ukr.J.Phys.Opt.2026.03069

Анотація. *Лазерне кільватерне прискорення є ефективним методом генерації та прискорення релятивістських електронних згустків. Параметри цих самоінжектованих згустків залежать від параметрів лазера та плазми. У цій роботі показано, що формування самоінжектованого згустку є чутливим до профілю лазерного імпульсу - драйвера. Автори порівняли імпульс із крутим переднім фронтом та імпульс із пологим переднім фронтом за всіх інших однакових параметрів лазера. Показано, що для імпульсу з крутим переднім фронтом формується самоінжектований згусток, тоді як для імпульсу з пологим переднім фронтом самоінжекція не спостерігається. Формування та подальше кільватерне прискорення самоінжектованих згустків досліджувалися в циліндричних і конічних плазмових каналах як для однорідних, так і для поздовжньо неоднорідних профілів плазми. Збільшення енергії самоінжектованого згустку було досягнуто в конічному каналі, а також у циліндричному каналі з неоднорідною плазмою.*

Ключові слова: *лазер, плазмовий канал, кільватерне прискорення, неоднорідна плазма, електронний згусток*